2016

Atmospheric Sensitivity to Roughness Length in a Regional Atmospheric Model Over the Ohio-Tennessee River valley

Rezaul Mahmood
University of Nebraska - Lincoln

Meteorol Atmos Phys (2016) 128:315–330
DOI 10.1007/s00703-015-0415-z

ORIGINAL PAPER

Atmospheric sensitivity to roughness length in a regional atmospheric model over the Ohio–Tennessee River Valley

Arturo I. Quintanar[2,3,4] · Rezaul Mahmood[1,2,3] · Astrid Suarez[1,2,3,5] · Ronnie Leeper[2,3,6]

Received: 6 December 2014 / Accepted: 19 October 2015 / Published online: 5 November 2015

Abstract The response of a regional atmospheric model to small changes in roughness length of two vegetation categories (crops and deciduous broadleaf forest) was analyzed for three synoptic events in June 2006. These were characterized by two convective events (June 11 and 22) and one prefrontal event (June 17). The responses of the model, for precipitation, equivalent potential temperature and wind field were notable in general. However, the response became muted as roughness lengths were increased or decreased. Atmospheric response to these changes varied for different convective events. A small dependence on roughness length was found for the sensible and latent heat fluxes and planetary boundary layer heights during the convective event of June 11. For the June 22 event, the model response was weaker for the crop-only and forest-only roughness length experiments compared to the response when both the crop and forest-only roughness length were changed in combination.

Responsible Editor: S. Hong.

✉ Rezaul Mahmood
rezaul.mahmood@wku.edu

[1] Meteorology Program, Western Kentucky University, Bowling Green, KY, USA

[2] Department of Geography and Geology, Western Kentucky University, Bowling Green, KY, USA

[3] Kentucky Climate Center, Western Kentucky University, Bowling Green, KY, USA

[4] Present Address: Centro de Ciencias de la Atmosfera, Universidad Nacional Autónoma de México, Mexico, Mexico

[5] Present Address: Department of Meteorology, Pennsylvania State University, University Park, PA, USA

[6] Present Address: Cooperative Institute for Climate and Satellites (CICS), North Carolina State University, Raleigh, NC, USA

1 Introduction

The model responses to changes in surface characteristics have been the subject of numerous scientific studies. This is because the processes that control flux of energy, mass, and momentum in the atmosphere are determined largely by the physical conditions of the surface (Oke 1987; Stull 1988). A large number of studies have investigated the impact of orography (Carruthers and Hunt 1990; Allen 2006), surface roughness (Lettau 1969; Pielke 1973; Thompson 1978; Garret 1982; Sud and Smith 1985; Dorman and Sellers 1989; Raupach 1994; Harman and Finnigan 2007; Finnigan et al. 2009), albedo (Charney et al. 1977; Sud and Smith 1984; Garratt 1993; Pitman et al. 2004), land use and land cover, and soil moisture (Avissar and Pielke 1989; Pielke et al. 2002; LeMone et al. 2008) on the atmosphere.

The present paper focuses on atmospheric sensitivity to surface roughness. In this vein, one difficult challenge has been the assignment of appropriate values of roughness length to the numerous elements that constitute roughness of the underlying surface (Grimmond and Oke 1999). Several avenues of research have been proposed to approach the problem from a combination of theoretical and observational techniques. The obvious one was to specify roughness length from profile methods or from single-point estimates (Sugita and Brutsaert 1992; Bottema et al. 1998; Eng and Brutsaert 2002; Grimmenes and Thue-Hansen 2004). Another method, pioneered by Lettau (1969), specified roughness length from the geometrical consideration of the roughness elements. He suggested a

parameterization of the momentum roughness length to be proportional to the ratio of the area presented to the wind and the specific area occupied per one unit roughness element. These geometric methods have been used in conjunction with geographic information systems to determine zero-plane displacement and roughness length (Grimmond and Oke 1999; Hassager et al. 2003). As a follow-up of this idea, the concept of effective roughness was used. In this case, roughness length of an element could be used as representative of a large area or it could be estimated from aggregation of roughness values for homogeneous areas (Claussens 1991; Hassager et al. 2003). Variants of these methods have been proposed but the degree of uncertainty associated with each technique has not been reduced significantly. Wieringa (1992) has revised a series of experimental studies only to find that roughness length estimates can vary significantly among each other up to a factor of 3. This situation is particularly evident in estimates of roughness length for vegetated areas and crops. Wieringa (1992) noted that the geometrical disposition of rows and their width as one source of uncertainty which can have an appreciable effect over acceptable values of roughness length. Additional examples of the role of surface roughness length in land–atmosphere interactions can be found in Harman (2012) and Weligepolage et al. (2012).

Spatial and temporal changes in roughness length can result in alterations of turbulent exchange coefficients and hence in changes to the sensible and latent heat fluxes at the surface. From the air quality point of view, uncertainty in roughness length can be a cause of uncertainty on the values of near-surface wind speeds and therefore significantly affect the trajectories of air parcels (Quintanar et al. 2009; Wu et al. 2009). Dry deposition fluxes of contaminants can also be affected by the uncertainty in roughness length since these are formulated in terms of aerodynamic resistances (De Ridder et al. 2004).

Relatively few regional atmospheric modeling studies have addressed the sensitivity to roughness length changes (Pielke 1973; Hassager et al. 2003). Thus, a detailed investigation of forecast sensitivity to roughness length is long warranted. It is particularly important to understand smaller changes or bias or error in surface roughness length and their impacts on the atmosphere. We may conceptualize these impacts based on our overall understanding of surface roughness–atmospheric relationships. However, the question that still needs to be addressed is 'what are the magnitudes of responses (quantitative examples) for small changes in surface roughness length under different synoptic states of the atmosphere?'

Hence, the objective of this research was to investigate and quantify atmospheric responses to small changes in surface roughness for two distinct vegetation categories, namely crops and woodland and deciduous broadleaf forests which comprise a significant portion of the vegetated surface of the Ohio River Valley. Three convective events from June 2006 were examined for this purpose. Moreover, the study was completed in support of an ongoing air quality work conducted by the authors.

2 Data and methodology

2.1 The model

In this research, the Penn State University/UCAR regional atmospheric model MM5 version 3.7.4, coupled to the Noah land surface model (LSM) was applied (see Chen and Dudhia 2001). The Noah LSM used four soil layers (10, 30, 60 and 100 cm in thickness) to predict soil temperature and soil moisture. The total soil depth was 2 m with the root zone in the upper 1 m. The Noah LSM communicated with the model atmosphere through a planetary boundary layer (PBL) model and a surface layer model that computed potential evaporation as described by Mahrt and Ek (1984). The PBL scheme chosen here was based on the work by Troen and Mahrt (1986), later coupled to the NCEP Medium-Range Forecast model (MRF-PBL) by Hong and Pan (1996). The MRF-PBL scheme supplied the Noah LSM and the surface layer model with values of stability-dependent (bulk) exchange coefficients, which were used to estimate sensible and latent heat fluxes at the surface. These energy fluxes were used in turn by the MRF-PBL to compute heating and moistening of the boundary layer (Chen and Dudhia 2001). Despite some shortcomings regarding overestimation of PBL heights and underestimation of surface wind fields, the MRF-PBL continued to be used because of its computational efficiency and similar performance compared to other more sophisticated PBL schemes (Cheng et al. 2003; Zhang and Zheng 2004).

The turbulent exchange coefficients for heat and moisture fluxes were functions of the momentum and the heat roughness lengths. These two roughness lengths differed in the current Noah LSM design (as of version 3.7.4) by the addition of a molecular resistance term to the heat roughness length, which effectively reduced the exchange coefficient for heat. Under this particular model version of MM5, the dependency of the exchange coefficient on roughness length was found to be rather weak for neutral conditions (see "Appendix" for additional explanation). However, in the event of strong coupling between the MRF-PBL scheme and the LSM, particularly during convective activity, the energy fluxes at the surface can be significantly altered and consequently, the dynamical and thermal evolution of the PBL as well.

In this study, sensitivity tests are conducted to investigate the impact of varying roughness lengths on model forecasts for two land-use categories: deciduous broadleaf forest (*F*) and cropland/woodland (*C*). The values of roughness lengths were provided at initialization time to the MM5 from a lookup table containing a USGS 24 land use category for summer. The changes in roughness length were made directly to the lookup table and maintained throughout the simulations.

For the coarse grid simulations, the Kain–Fritsch cumulus convection parameterization scheme incorporating a shallow convection scheme was selected (Kain 2004). For higher resolution simulations the cumulus convection parameterization was not used. Finally, for the cloud microphysics representation, the simple ice microphysics of Dudhia (1989) was chosen.

2.1.1 Domain configuration

The model simulations were performed with two domains in a one-way interaction mode. Figure 1 shows the outer domain with horizontal grid spacing of 12 km, covering a 1600 × 1000 km region of the South Central U.S., and the inner domain with horizontal grid spacing of 4 km, covering a 800 × 500 km region of the Ohio River valley centered over Kentucky. Both domain projections (Lambert conformal) were centered at 37.1 N, 86.7 W in south central Kentucky. The modified *C* and *F* categories were only implemented in the inner domain (4-km grid spacing). Hence, a one-way interaction mode between the outer and inner domain was needed to isolate the lateral forcing of the outer domain from the effects of roughness length changes. The dates of simulation were chosen to coincide with three periods in June 2006 when an air quality measuring campaign in Logan County in south central Kentucky was conducted.

Both model domains are configured with 31 vertical levels and 13 half-sigma levels below the 0.85 level, decreasing from 1.0 to 0.88 in intervals of 0.01. This roughly corresponded to a vertical grid spacing of 90.0 m up to the 0.85 sigma level. The lowest computational level was set at 0.995, roughly corresponded to a height of about 35 m above the ground.

2.1.2 Anomaly experiments

The MM5 is initialized at 1200 UTC (0600 LST) for three synoptic events on June 11, 17 and 22, 2006 and integrated for 24 h. Both, the MM5 and the Noah LSM were initialized with NCEP Final Reanalysis data (FNL) at 1° × 1° horizontal resolution and updated every 6 h (http://dss.ucar.edu/datasets/ds083.2/ as obtained from the Research Data Archive at the NCAR/UCAR website). These data sets include soil moisture data at the same four soil levels mentioned previously for the Noah LSM. Additional high resolution (30 s) land use land cover data was provided from a 25 category USGS data archive used by the TERRAIN interpolation stage of MM5 to the model's computational grid (Zehnder 2002).

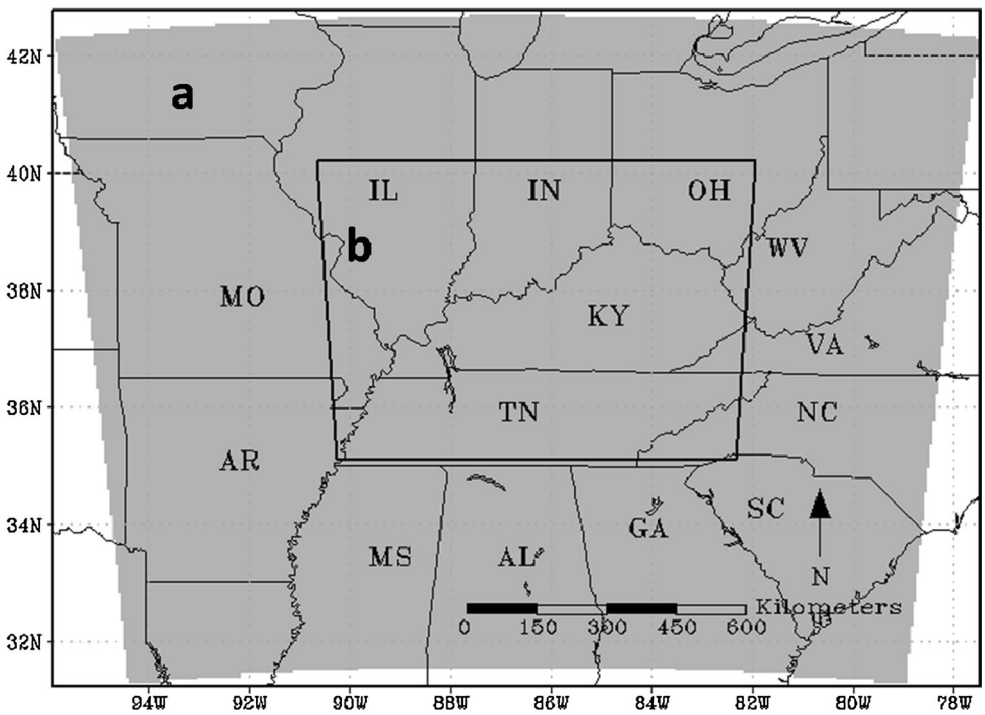

Fig. 1 Model domains *a* outer domain grid spacing at 12 km and *b* inner domain grid spacing at 4 km

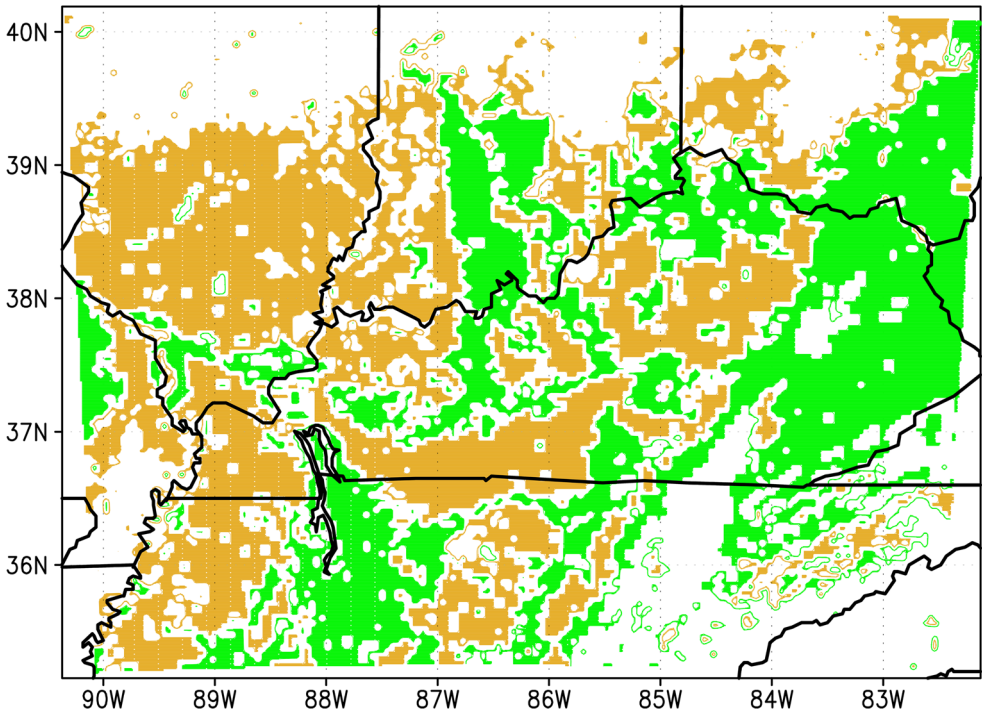

Fig. 2 USGS land use land cover map for crops/woodland mosaic (in *light brown*) and deciduous broadleaf forest (in *green*). Roughness length for crops is set in the CTRL simulation to 0.2 and to 0.5 m for the deciduous broadleaf forest categories

In the control (CTRL) run, the values of roughness length for the *C* and *F* land use categories were set to the standard values used in MM5 runs, namely, 20 and 50 cm, respectively. Figure 2 shows the area covered by the *C* and *F* categories, respectively. The *C* category could be found over parts of south, central and northern Kentucky. It also occupied wide areas over Illinois, Missouri, and western and central Tennessee. The area covered by the *F* category was clearly smaller with respect to its *C* counterpart and was found mostly over eastern Kentucky and smaller portions of southern Indiana and western Tennessee. The *C* and *F* areas covered about 40 and 30 % of the computational domain, respectively.

In the anomaly experiment runs, the roughness length value of one category was changed from that in the CTRL simulation in steps of 5.0 %, from −25.0 up to 25.0 % (i.e., a total of ten experiments for each category change) while keeping the roughness length of the remaining category at the CTRL value. As noted above, in the land cover dataset, roughness length is 20 cm for crops. Hence, 5 % changes (increase or decrease) would result in roughness length of 19 or 21 cm while 25 % changes would result in 15 or 25 cm roughness length. Because of this reason, other researchers (e.g., Sud et al. 1988) made several orders of magnitudes of changes to demonstrate the impacts of changes in roughness length. However, impacts of small changes remained relatively less understood. This study, in fact, provided a quantitative estimate of impacts of these small changes and uncertainties.

Since both *C* and *F* land categories covered adjacent regions it became important to assess the response of the model when these two roughness length values were changed simultaneously in steps of 5.0 % while keeping the sign of the change equal in both *F* and *C* categories. We referred to the combined changes in both categories of roughness length as *CF*. Thus, a total of 70 roughness length change experiments were performed which was a subset of the 120 all possible anomaly experiments per synoptic event. The analysis of this smaller sample was considered sufficient to obtain first order effects of roughness length changes upon the model's atmospheric state. To identify and analyze the response of the model, the ensemble averages of pertinent atmospheric variables over the anomaly experiment realizations and the time and area averages of individual experiment realizations were performed. We denoted the 5-member ensemble averages of simulations that have an increase in roughness length from CTRL as CUP and FUP for the crops/woodland and deciduous broadleaf categories, respectively. Similarly, we used CDN and FDN when roughness lengths were decreased. When both categories were changed in combination they were denoted by CFUP and CFDN. Consequently, the 10-member ensemble averages were denoted as CEN, FEN and CFEN. To identify individual experiment realizations the notation CDNxx, CUPxx, FDNxx, FUPxx, CFDNxx, CFUPxx, were used, where xx was replaced by 05, 10, 15, 20, and 25 to indicate the percentage change from CTRL values.

In the following sections, the model's response to changing roughness length for the deciduous broadleaf and crop/woodland land use categories was analyzed for the three different events, June 11, 17 and 22 2006, as mentioned above. Precipitation, equivalent potential temperature (θ_e), the near-surface horizontal wind field at the sigma level 0.975 (the area average pressure is approximately 980 hPa at this level for all experiments), the latent and sensible heat fluxes and the PBL height were examined for each of the three synoptic events. The time periods used to perform the averages and the accumulation of precipitation values were taken from 1800 UTC for June 11, 17 and 22 to 0600 UTC of the next day (1200 LST to 0000 LST). This model integration period included the last 12 h of simulation from 1200 LST to 2300 LST and included the most relevant convective events. Results and discussion of model output was restricted to the inner domain (4 km resolution).

3 Results

3.1 Synoptic conditions and control simulations

Figure 3a shows the June 11 2006, 12-h modeled accumulated precipitation fields and the 980 hPa ($\cong$0.975 sigma) 12-h average horizontal wind field for the CTRL simulation. Figure 3b shows the corresponding fields from the North American Regional Reanalysis (NARR) (Mesinger et al. 2006). During this time period, a weak cold front traversed the study area and set off showers over much of Kentucky and Tennessee. The overall trend in accumulated precipitation was well captured by the model with a tendency to overestimate maximum rainfall by about 10–20 mm in narrow precipitation bands over central Kentucky. The near-surface wind field patterns were also reasonably well captured in magnitude ranging from about 2.0–4.0 m s^{-1}. South-westerly winds over Tennessee and north-easterly wind over the northeast of Kentucky were reproduced well by the model. However, the cyclonic center is placed about 2.5° to the west of that seen in the NARR data (Fig. 3a).

Figure 3c, d shows the same fields as in Fig. 3a, b but for June 17 (June 17 1800 UTC to June 18 0600 UTC), characterized by prefrontal convection. During this 12-h period, precipitation was initiated from localized convective activity east of the Mississippi river over western Kentucky and Tennessee. Precipitation values from the NARR data set exceeded 40 mm in this region (Fig. 3d). The model underestimated precipitation by about 30 mm and placed higher precipitation rate values to the northwest of the study area over Illinois (Fig. 3c). Model simulation and NARR data show southerly winds with speeds of about 2.0–4.0 m s^{-1} over much of the study region.

Figure 3e, f show precipitation and wind fields for the June 22 event (June 22 1800 UTC to June 23 0600 UTC). In this case, a slowly propagating stationary front traversed the study area, with precipitation accumulated over eastern and central Kentucky and the Ohio River in northern Kentucky, Illinois and Indiana (Fig. 3f). Modeled precipitation in excess of 30 mm was found over the northwest corner of the study area over Illinois with lower than observed values by about 10–20 mm to the northeast over Kentucky, Indiana and Ohio. Winds are predominantly south-westerly over much of the region and northerly in the northwest part over Illinois and Indiana, as shown by the NARR data set. The model captured the wind field distribution satisfactorily except over central Kentucky, along the Kentucky-Tennessee border, and around the northern and southern border of the domain. Over Illinois, modeled winds had a strong northerly component unlike the north-westerly flow depicted in the NARR data.

Despite some uncertainty with respect to location and initiation of modeled precipitation for June 17 and June 22, it was pertinent to assess the impact of roughness length changes on the thermodynamics and the overlying circulation within the boundary layer. This assessment was particularly useful since this study was complementary to one in which anomaly experiments with soil moisture changes have been conducted for the same time periods and computational domain (Quintanar et al. 2009). The objective of the present study was to obtain information about the sensitivity of the model to roughness length.

3.2 11 June 2006

3.2.1 Precipitation, wind and thermal response

Figure 4a, b show differences of precipitation, equivalent potential temperature, and horizontal wind field. In particular, Fig. 4a shows the differences in the 0.975 sigma level 12-h average horizontal wind field and the 12-h accumulated precipitation between the CTRL and the ensemble CFEN, (CTRL−CFEN). The precipitation differences were characterized by narrow bands to the west and central portions of Kentucky with positive values exceeding 25 mm. The larger response in the horizontal wind field of about 1.0–2.0 m s^{-1} is seen to be co-located with larger changes in precipitation. Close inspection of the maps revealed almost identical horizontal patterns for precipitation and wind field differences for (CTRL−CEN) and (CTRL−FEN) (both not shown) and (CTRL−CFEN) ensembles. The 24-h time evolution of the *domain average* accumulated precipitation differences for each member realization (not shown) revealed that the values of precipitation differences were very small (in the order of 0.1 mm or less). This was because of cancelation of positive and

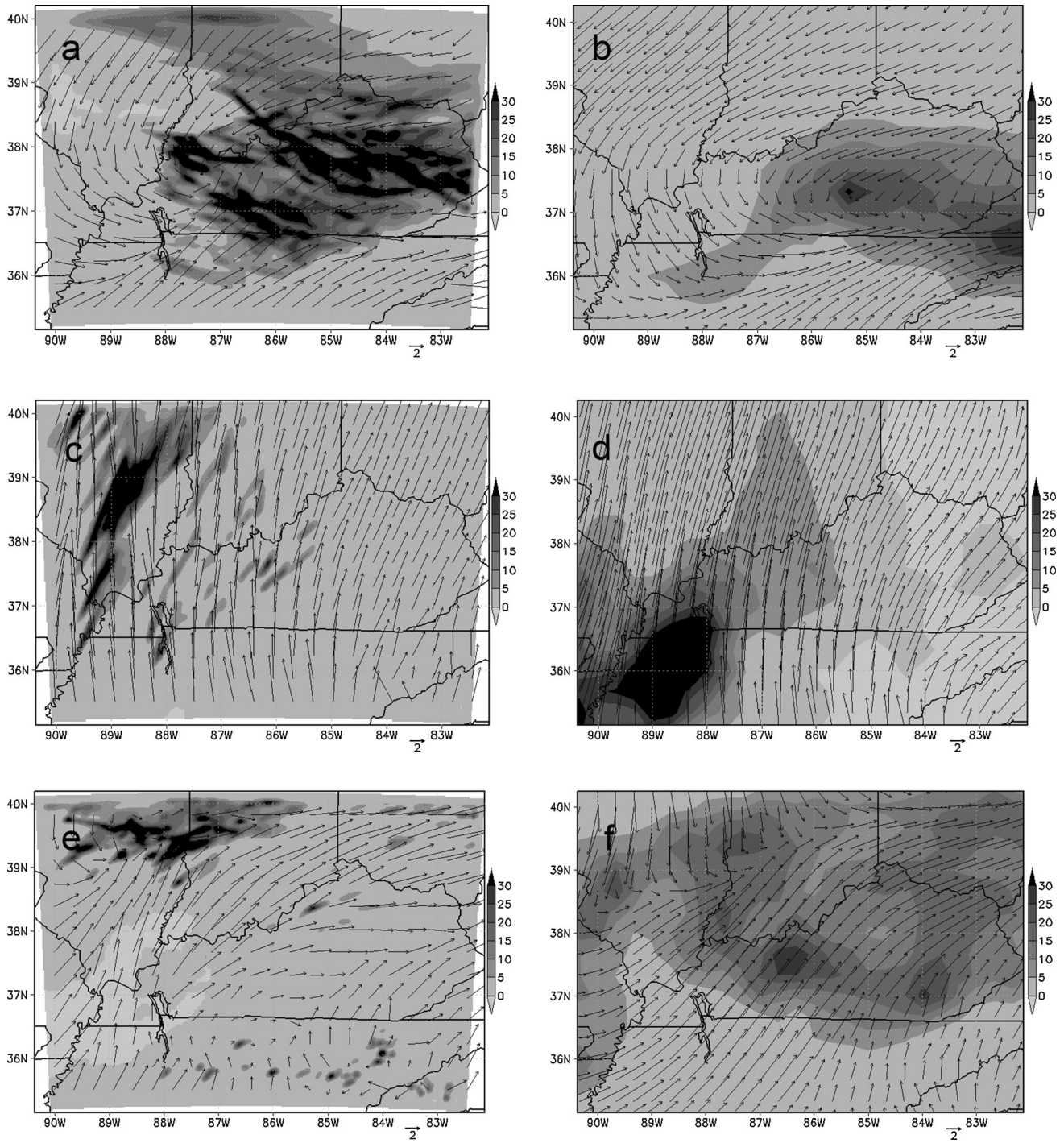

Fig. 3 **a**, **c**, **e** 12-h accumulated precipitation (mm) and 975 mb horizontal wind field from control model simulation, respectively; and **b**, **d**, **f** from NARR on June 11 (June 11 1800 UTC–June 12 0600 UTC), June 17 (June 17 1800 UTC–June 18 0600 UTC), and June 22 (June 22 1800 UTC–June 23 0600 UTC), respectively

negative anomalies over the computational domain, as could be seen from inspection of the gray and white areas in Fig. 4a. The result was consistent with the horizontal patterns of precipitation differences exhibited in the ensemble averages for *C*, *F*, (not shown) and *CF* (Fig. 4a).

It is conceivable that, given the geographical distributions of *C* and *F* categories over the study region (for instance, *C* is dominant over Illinois, see Fig. 1), a pattern of shifted precipitation concomitant with a change of surface wind speeds might be discerned over regions where

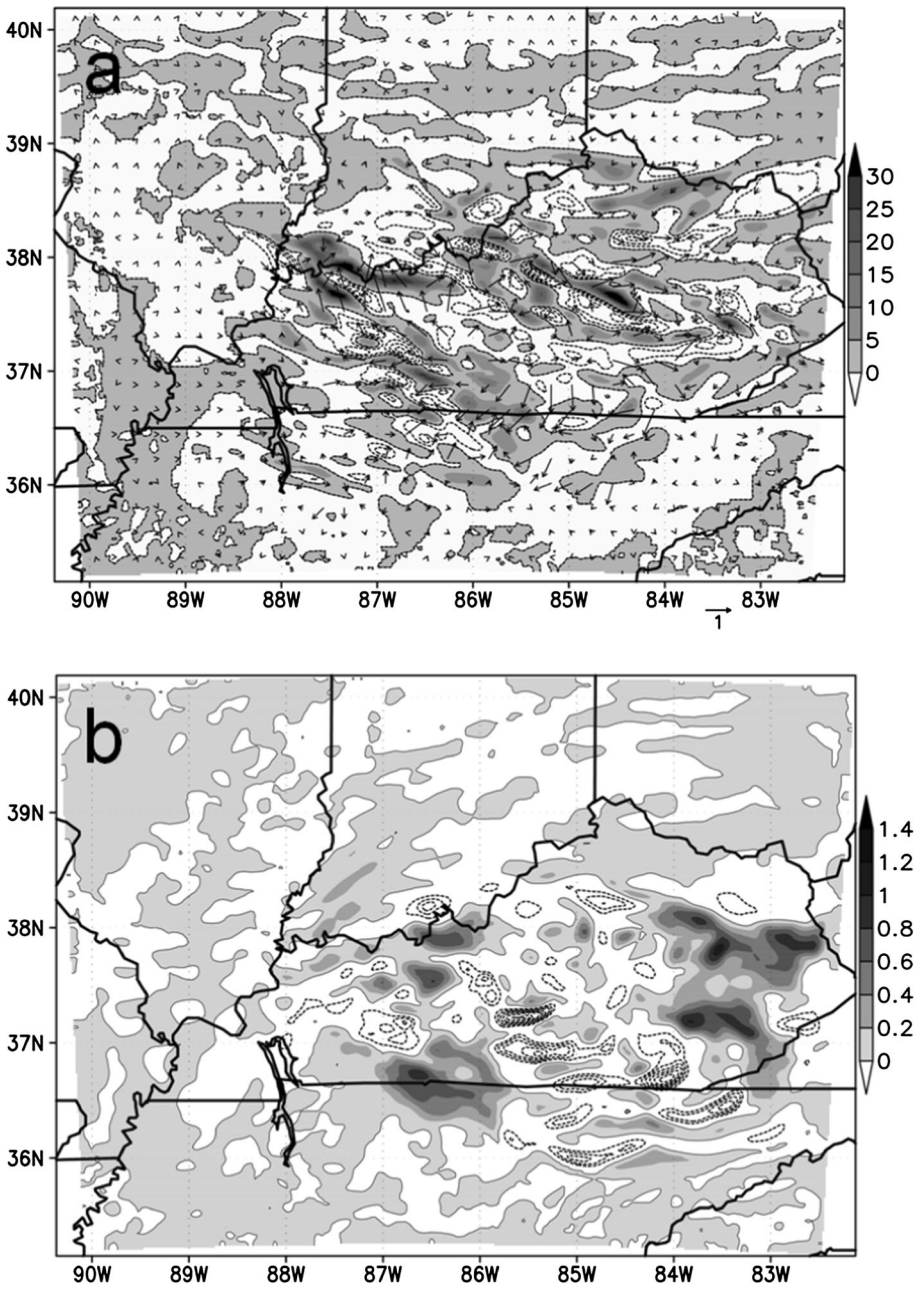

Fig. 4 **a** June 11 ensemble differences in 12-h accumulated precipitation (mm) and the 12-h average horizontal wind field for (CTRL−CFEN). Contour interval for *dashed lines* of precipitation is −5 mm or less. **b** Similarly, for equivalent potential temperature (K) at the 0.975 sigma level. Contour interval for *dashed lines* is −0.2 K or less

larger horizontal gradients of roughness length are located. To explore this possibility further, two experiments (not included in the suite of experiments for this study) were performed whereby differences in roughness length between two adjacent areas of forests (*F*) and crops (*C*) are maximized. The experiments in our notation are: FUP25_CDN25 and FDN25_CUP25. Comparisons with the CTRL simulation and between them reveal very similar patterns of shifting precipitation and surface wind field as those found in the previously shown Fig. 4a for the June 11 case (not shown). The June 17 case, showed similar patterns of shifting precipitation over Illinois regardless of how the *C* and *F* roughness length categories were changed. It is intriguing why precipitation changes tend to cluster around larger values of precipitation, without a preferential direction in roughness length changes. This question needs to be addressed in a future study.

Figure 4b showed θ_e changes at sigma level 0.975. For (CTRL−CFEN) it was found that differences in θ_e was of the order of 0.0–0.5 K outside the region where convection took place in Kentucky. Inside the region of largest convective activity, differences in θ_e attain values of up to 3 K. As shown above, in the case of precipitation differences, the horizontal patterns of θ_e were almost identical to (CTRL−CEN) and (CTRL−FEN) (both not shown). The horizontal pattern of θ_e differences showed colder and drier

air in eastern and south-western Kentucky for the CEN, FEN and CFEN ensembles, while moister and warmer air in central Kentucky. From the results it became evident that the local change in roughness length for the *C* and *F* categories impacted the entire domain. It is different from impacts of soil moisture changes where only upwind or downwind regions experienced these modified θ_e (Quintanar et al. 2008; McPherson and Stensrud 2005).

In addition, the area-averaged results for the *F*, *C* and *CF* land categories show very similar patterns in amplitude and time evolution. Hence, the results presented here are only for the *F* category. Figure 5 shows the time series of area-averaged accumulated precipitation for the CTRL simulation on 11 June, 2006 for the deciduous broadleaf forest *F* category (blue line). Precipitation increases from near zero in the first 12 h of simulation to about 12.0 mm by the second 12 h. Additionally, the area average of the standard deviation from the CTRL is calculated using the ten anomaly experiments (FUPxx, FDNxx as described above in Sect. 2.1.2) and plotted as an error bar. The standard deviation increased from near zero at beginning to about 3.4 mm near the end of the simulation. This indicates the evolution of larger spatial variability of anomaly experiments over time. The standard deviation for all three cases seemed controlled by the strength of synoptic conditions. In the June 11–12 case, synoptic forcing is the smallest of the three cases (please see Fig. 7b in the manuscript) and, while area-averaged precipitation did increase from changes in roughness length values, it is unclear how this induced variability at daily time-scales is internal to the model. Percentage-wise, in this case, the standard deviation remained almost unchanged up to the end of the simulation. June 17–18 and June 22–23 cases show behavior analogous to the June 11–12 case.

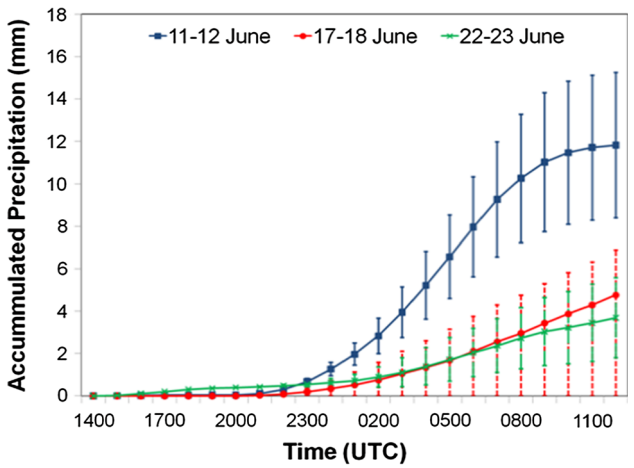

Fig. 5 Time series of hourly area average accumulated precipitation (mm) for three events for broadleaf forest. *Error bars* show spread of precipitation

3.2.2 *Vertical cross section*

The vertical distributions of differences in θ_e and vector wind field are shown in Fig. 6 for a north–south cross

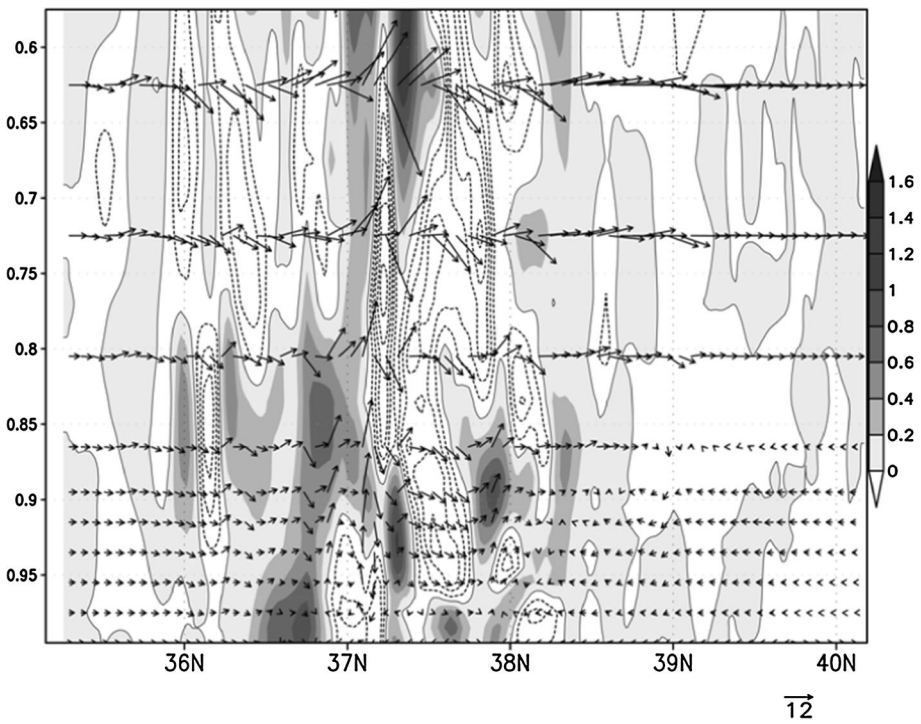

Fig. 6 South–north vertical cross section (at 86.7°W) for differences of equivalent potential temperature and meridional and vertical wind components. Contour interval for *dashed lines* is 0.2 K

section placed at 86.7°W. The largest differences in θ_e extended from the surface through much of the mixed layer (see Fig. 6). Generally, larger wind differences were co-located with larger differences in θ_e, ascending motion in the region of positive differences (shaded area), and descending motion over regions of negative differences (white areas). Again, this contrasts with studies where soil moisture changes resulted in either solenoidal (Leeper et al. 2009) or single-cell circulation throughout the mixed layer (McPherson and Stensrud 2005).

3.2.3 *Near-surface wind field response*

Domain average zonal and meridional wind and friction velocity for *CF* are presented in Fig. 7a–c. In the CTRL simulation, the zonal wind component increased up to about 1.5 m s^{-1} during the first 12 h (1200–0000 UTC) of simulation and then decreased to −0.75 m s^{-1} during the following 12-h period (0000–1200 UTC; Fig. 7a). Anomaly experiments show very small (nearly zero) deviation from CTRL during the first 12 h of simulation. However, deviations became more prominent during the second 12 h period (Fig. 7a).

CTRL meridional wind also shows, generally, similar changes over time (Fig. 7b). However, magnitude of change in (absolute term) was more prominent for zonal wind during the first 12 h, while meridional winds dominated the second 12 h period. In addition, magnitudes of deviations were nearly similar for meridional wind during second 12 h of the anomaly experiments. Like zonal wind, first 12 h did not show any deviations from the CTRL.

Friction velocity for CTRL simulation increased during the first 6 h of simulation and then started to decline slowly (Fig. 7c). However, it declined rapidly before stabilized during the last and first hours of initial and second 12 h segments of simulation. Deviations from CTRL were smaller during the first 12 h of simulations while they were much larger during the second 12 h. This is related to the increase in simulated convective activity concomitant with larger horizontal convergence at lower levels from CTRL.

Additional analysis of domain average differences of CTRL−CFDN and CTRL−CFUP for the zonal wind components at 10 m were shown in Fig. 8a. The difference reached a maximum value of about 0.08 m s^{-1} in absolute value for the largest changes in roughness length (CFDN25 and CFUP25) at around 2200 UTC on June 11 and about 0.12 m s^{-1} at 0800 UTC on June 12. A similar behavior was found for the meridional wind component (not shown) except the range of changes was slightly larger than those found for the zonal wind component later on June 12 (0600 UTC). Larger differences in the horizontal wind vector at 10 m (not shown) were also found around areas of large differences in precipitation as was shown for its

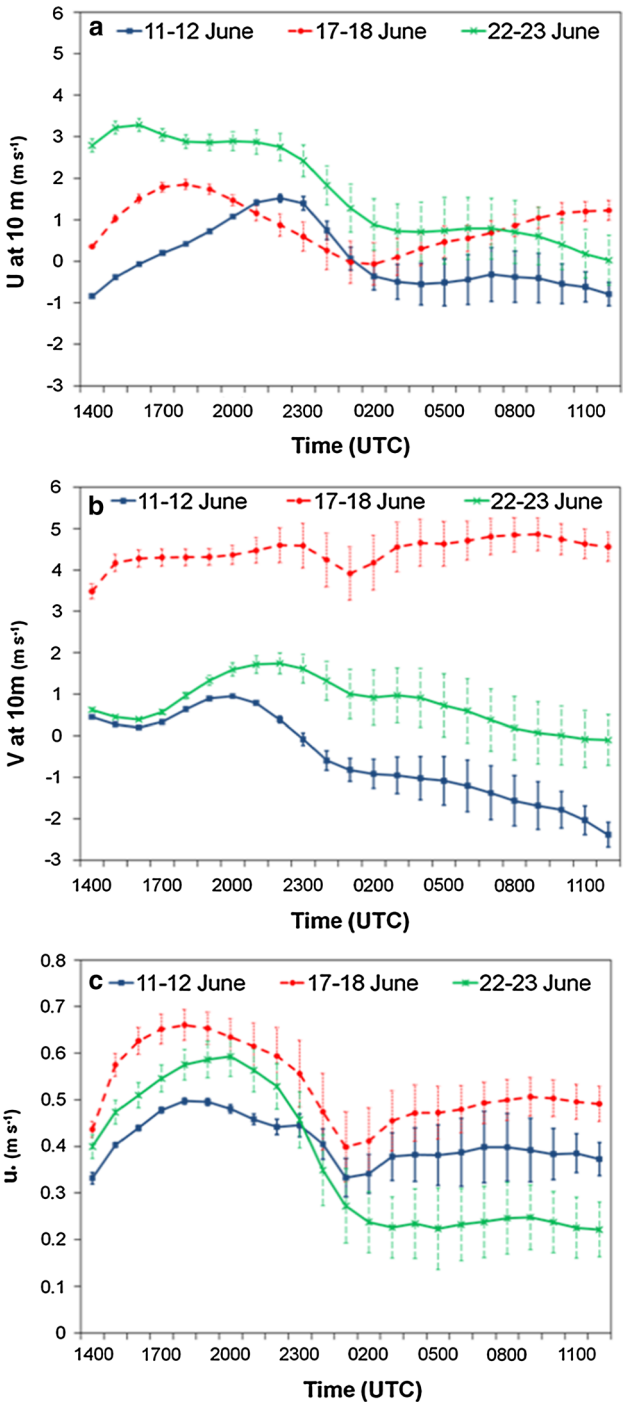

Fig. 7 Time series of domain average for the CTRL simulation for **a** zonal wind, **b** meridional wind and **c** friction velocity (u_*). *Error bars* are area averages of standard deviations of anomaly experiments from the CTRL

counterpart at the 0.975 sigma level (see Fig. 4a). It was noted that, for a period between 1200 and 1800 UTC, the zonal wind component in area average sense decreased from CTRL values when roughness length is increased (dotted lines in Fig. 8a). Conversely, it increased when

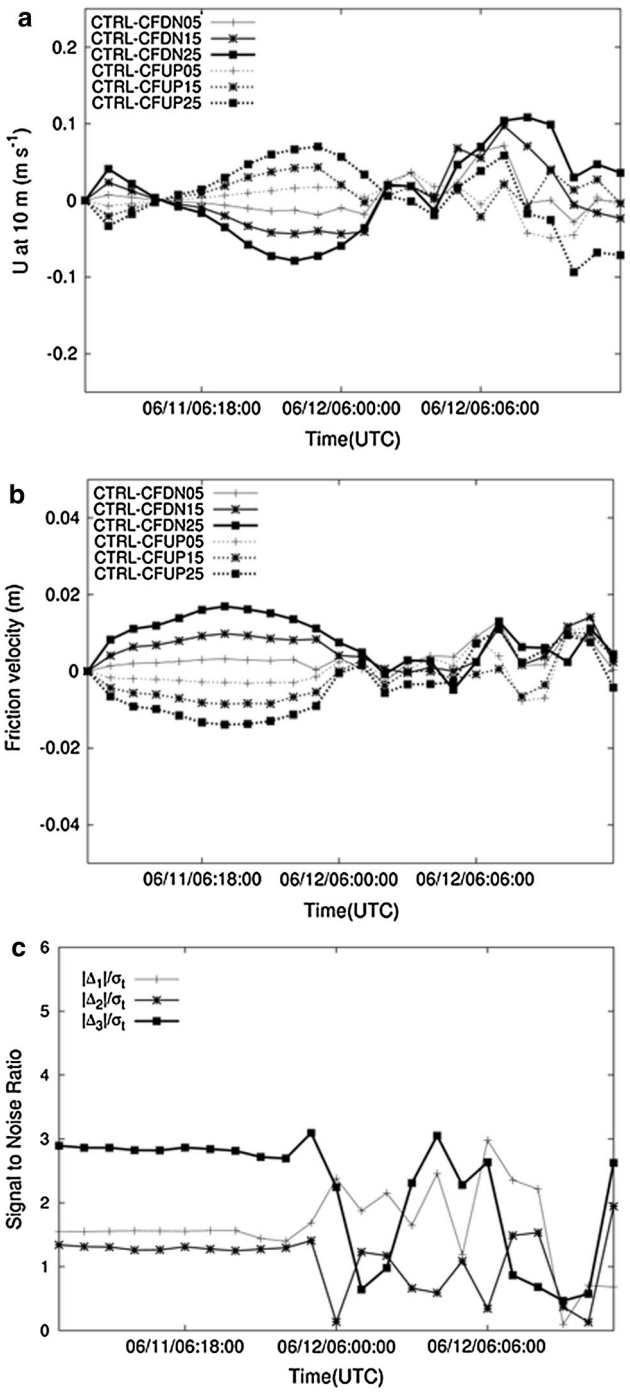

Fig. 8 June 11 time series of domain average horizontal differences for (CTRL−CFDN) and (CTRL−CFUP) of **a** zonal wind component U_{CTRL} at 10 m, **b** friction velocity as a function of selected momentum roughness length percent changes, **c** signal to noise ratio for the zonal wind component at 10 m, $|\Delta_1| = |U_{\mathrm{CTRL}} - U_{\mathrm{CFDN25}}|$, $|\Delta_2| = |U_{\mathrm{CTRL}} - U_{\mathrm{CFUP25}}|$, $|\Delta_3| = |U_{\mathrm{CFUP25}} - U_{\mathrm{CFDN25}}|$ and the time-dependent standard deviation σ_t

roughness length was decreased (black lines in Fig. 8a). The corresponding differences in friction velocity were shown in Fig. 8b. In this case, as roughness length was increased (decreased) friction velocity increased (decreased) due to a rougher (smoother) surface consistent with a higher (lower) surface stress. The behavior shown in Fig. 8a for the zonal wind component was explained from the logarithmic wind profile for neutral conditions.

Figure 8c, showed the signal-to-noise ratios $|\Delta_1|/\sigma_t$, $|\Delta_2|/\sigma_t$ and $|\Delta_3|/\sigma_t$ for the domain average zonal wind component at 10 m (U), where the numerator is the absolute value of $\Delta_1 = U_{\mathrm{CTRL}} - U_{\mathrm{CFDN25}}$, $\Delta_2 = U_{\mathrm{CTRL}} - U_{\mathrm{CFUP25}}$, $\Delta_3 = U_{\mathrm{CFUP25}} - U_{\mathrm{CFDN25}}$ and σ_t is the variance as function of time obtained from the ten anomaly roughness experiments. To estimate of the significance of the response, the procedure by Chervin and Schneider (1976) was used (please refer to eqs. 2 and 3 in their paper). The number of degrees of freedom is 9 (one control and ten experiments minus 2) which at 95 % confidence level requires the signal-to-noise ratio to be larger than 3.196 (see Chervin and Schneider 1976, pp. 411) to dismiss the null hypothesis for a two-tailed Student t test. For a 90 % confidence level the ratio needed to be larger than 2.592. Inspection of Fig. 8c revealed that (CFUP25−CFDN25) can be significant at the 90 % level except for several periods [0000–0300 UTC (1900–2200 LST), 0500 UTC (0000 LST) and 0700–1000 UTC (0200–0500 LST)]. On the other hand, differences between CTRL−CFDN25 were significant at 90 % level for a brief period in the early morning [0600 UTC (0100 LST)] whereas the difference CTRL−CFUP25 did not show any significance above the 90 % level for almost the entire day. The t test indicated, in this case, that probably a larger sample is required to achieve larger statistical significance. Despite this statistical fact it was interesting to find that the signs of differences in friction velocity and zonal wind speed are those expected on physical grounds at least during the first 12 h of this event.

3.2.4 *Planetary boundary layer heights and surface fluxes*

Figure 9a–c shows the time series of the domain average differences (vs. CTRL) of sensible and latent heat fluxes for each roughness anomaly experiment in the F category. The F experiment had been chosen because progression of its behavior was very similar to the other experiments. Sensible heat flux differences ranged from −0.2 to 0.7 W m^{-2} while for latent heat flux, differences ranged from −1.0 to 1.5 W m^{-2}. Between 1800 UTC and 2100 UTC, differences in sensible and latent heat changed from positive values (CTRL values larger than CDN, FDN and CFDN) to negative (CTRL values smaller than CUP, FUP, and CFUP) as percentage roughness length changes from −25 to 25 %. Hence, sensible and latent heat fluxes increased with increasing roughness length. This behavior in surface energy fluxes was partly explained from the

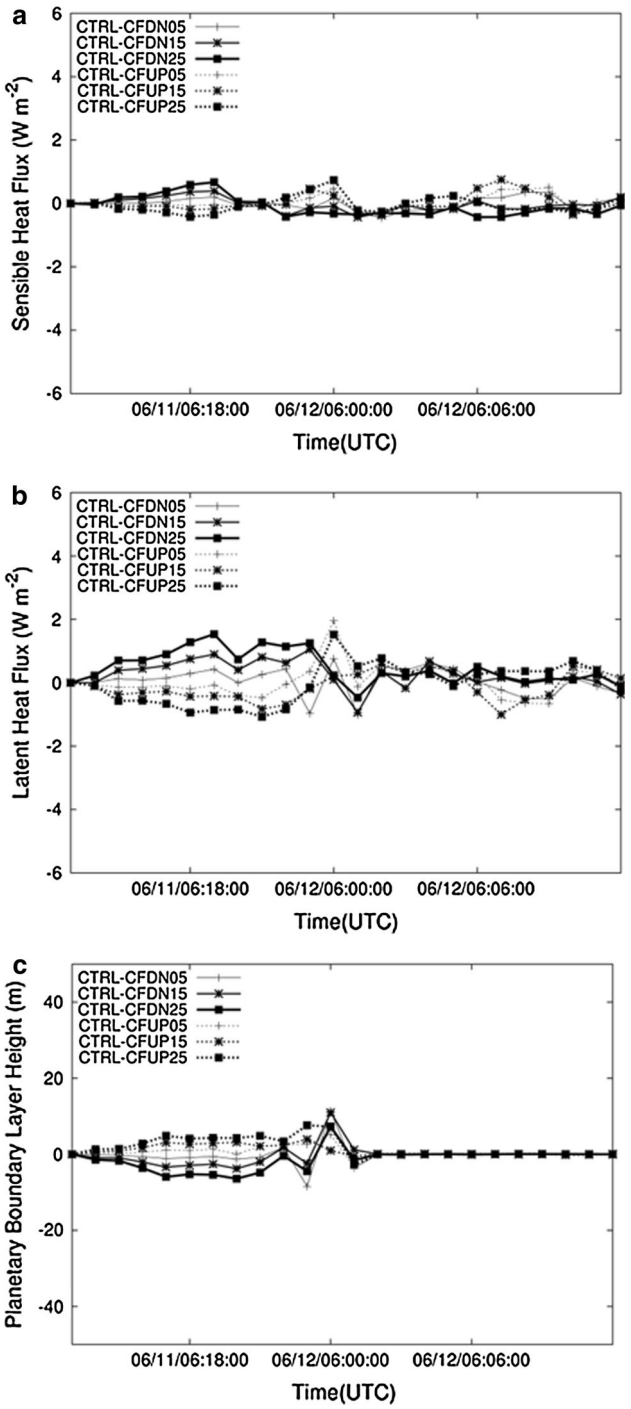

Fig. 9 June 11 time series of differences of (CTRL−CFDN) and (CTRL−CFUP) experiments **a** domain average sensible heat flux and **b** domain average latent heat flux and **c** domain average planetary boundary layer height

percentage change of the turbulent exchange coefficient to roughness length change. From the expression of the turbulent exchange coefficient for neutral conditions (Eq. 26 of Chen and Dudhia 2001) and assuming equality for both roughness length and heat roughness length, the percentage change for the *C* and *F* categories in the turbulent exchange coefficient was about 0.4 times the percentage change in roughness length (see "Appendix"). Close inspection of Fig. 9a for 1800 UTC showed that sensible heat flux decreased by about 0.58 W m^{-2} from the CTRL for a −25 % roughness length change, and up by 0.42 W m^{-2} from the CTRL for a +25 % change. Hence, the sensible heat fluxes increased by about 1.0 W m^{-2} as roughness length increased 50 %. The value of sensible heat flux at a −25 % change was 170 W m^{-2}. Thus, the percentage change for sensible heat flux was about 0.6 %. Similarly for latent heat fluxes, Fig. 9b shows 1.27 and 0.94 W m^{-2} decrease and increase for a −25 and 25 % changes, respectively, at 1800 UTC in latent heat fluxes. There was a net increase of about 2.2 W m^{-2} for an increase of 50 % in roughness length. In addition, there was 0.5 % increase in latent heat fluxes for a −25 % change in roughness length. These percentage changes in sensible and latent heat fluxes were too small to be explained from the computed sensitivity of the turbulent exchange coefficient. LeMone et al. (2008) also found very small changes in sensible heat fluxes for 30 % decrease in roughness length for grasses. They have explained that the effect of decreasing roughness length was compensated by a decrease in friction velocity and an increase in the heat roughness length. In other words, flux changes were not proportional to the roughness length changes. Further assessment of the model showed that this disproportionate response was linked to sensitivity of the exchange coefficient for the roughness parameterization (Please see "Appendix" for additional explanation). Despite the results, it was very interesting to find that, at least for June 11 event, at 1800 UTC the increasing change in surface fluxes corresponded to the increasing change in roughness length. This behavior was short lived. After 0000 UTC, the signs of the differences reversed for all experiments and the previous dependence with roughness length change was lost. The ensemble average for, both sensible and latent heat fluxes in CEN, FEN and CFEN resulted in estimates less than 0.5 W m^{-2} in absolute value due to cancelation among members of the ensemble (not shown).

The time series for the PBL height differences were shown in Fig. 9c. Positive differences of up to 5 m were observed for CFUP25 and negative differences of −5.3 m for CFDN25 between 1800 UTC and 2100 UTC. Differences in PBL height change from negative (CTRL values smaller than CFDN experiments) to positive (CTRL values larger than CFUP experiments) as roughness changes went from −25 to +25 % change. In other words, as roughness length changes from −25 to +25 %, PBL height decreases. This condition is rather unexpected given the observed increase in sensible heat flux in the anomaly experiments. However, other factors such as the stability of the model

atmosphere need to be factored in. In the MM5, PBL height is a function of stability conditions through the computation of a bulk Richardson number at every vertical level (Hong and Pan 1996). The change in roughness length not only affects the surface energy fluxes, but also affects the momentum transport into the atmosphere that can potentially change horizontal wind convergence of moisture which in turn can change the stability of the atmospheric column. Additionally, as found earlier, differences in sensible heat fluxes are perhaps too small to account for the PBL height behavior.

3.3 17 June 2006

3.3.1 Precipitation, wind and thermal response

As done for June 11, differences in the 0.975 sigma level 12-h averaged horizontal wind field and the 12-h accumulated precipitation between the CTRL and the ensemble and CFEN were analyzed (not shown). Large positive precipitation differences of up to 20 mm were observed over the northwest corner of the computational domain. Conversely, relatively small precipitation differences of about 5 mm or less were present over the central part of the domain. These differences were characterized by precipitation bands oriented in a south-west to north-east direction following the southerly mean-wind as in the control simulation (Fig. 3c). Negative precipitation differences were smaller (up to 10 mm). The domain average of these values for the individual ensembles (not shown) showed slightly reduced differences compared to its June 11 counterpart with differences of about 0.1 mm after 1200 LST. In addition, the model conserved domain average precipitation as found earlier for the June 11 case.

Again, Fig. 5 shows the time series of area-averaged accumulated precipitation for the CTRL simulation for 17 June, 2006 for *F* category (red line). As in 11 June, precipitation increases from near zero in the first 12 h of simulation to about 4.7 mm by hour 1200 UTC of 18 June at the end of the simulation. The standard deviation is shown to increase from near zero values to about 2.1 mm near the end of the simulation. Precipitation estimates were lower compared to the 11 June event and is consistent with Fig. 3c.

It was also found that a larger response in the horizontal wind field was co-located with larger changes in precipitation with speeds of up to 2.0 m s^{-1}. Once again, the close similarity of precipitation and wind field differences among the members of the ensemble average was verified and thus the lack of sensitivity to different magnitudes of roughness length changes was confirmed as well.

The differences in θ_e for (CTRL−CFEN) at 0.975 sigma level were approximately 3.0 K over Illinois and Indiana and less than 0.2 K over Kentucky. Hence, θ_e for the CEN, FEN, and CFEN ensembles show cooler, drier air over a large portion of the domain, particularly over Indiana and warmer, moister air over Illinois and the Indiana-Kentucky border. The similarity of pattern for θ_e among the ensemble differences (CTRL−CEN), (CTRL−FEN) (not shown) and (CTRL−CFEN) is verified in this event as well.

3.3.2 Vertical cross section

The vertical structure of differences in θ_e and wind vector field (meridional and vertical components) for a north–south vertical cross section located at 86.7°W were analyzed (not shown). The larger differences in θ_e were found near the surface and continued vertically throughout the mixed layer. Larger wind differences were co-located with larger differences in θ_e as observed before. However, vertical velocities were much weaker than those in June 11 event and no clear pattern of upward and downward vertical velocities was observed as in the June 11 event.

3.3.3 Near-surface wind field response

For the CTRL simulation, the zonal wind component increased up to 1.8 m s^{-1} during the first 12 h (1200–0000 UTC) of simulation after reaching a minimum of about 0.0 m s^{-1}. Subsequently, it approached 1.0 m s^{-1} during the following 12 h period (Fig. 7a). Anomaly experiments show very small (nearly zero) deviation from CTRL during the first 12 h of simulation. However, deviations became more prominent during the second half (last 12 h period) of the simulations (Fig. 7a).

CTRL meridional wind shows no appreciable tendency over time with values of about 3.0–4.0 m s^{-1} over the entire 24-h period (Fig. 7b). In the first 12 h, magnitudes of deviations were small for anomaly experiments and increased later during the second 12 h period.

Friction velocity for CTRL simulation increased during the first 6 h of simulation and then started to decline slowly (Fig. 7c). However, during the last and first hours of first and second 12 h segments of simulation, respectively, it declined rapidly and then stabilized. Deviations from CTRL were smaller during the first 12 h of simulations while they were much larger during the second 12 h.

In addition, CTRL−CFEN differences in the domain average zonal wind component at 10 m were found to peak at about 1800 UTC on June 18 with values of about 0.07 m s^{-1} (not shown). In contrast to the June 11 case; however, little or no variation was observed among the individual ensemble members in the first 12 h of the simulation. During the second 12 h of experiments, slight differences among the anomaly experiments appeared with no clear indication of a regular dependence on roughness

length changes. Friction velocity showed a similar pattern as its zonal wind counterpart. Closer inspection of friction velocity (not shown) revealed very small changes (on the order of 0.0005–0.001 m s^{-1}) as roughness length was changed.

The statistical significance test was evaluated as in the previous June 11 case. Here, it was observed that values of signal-to-noise ratios were exceedingly large (about 100–1000) early in the day. This occurred because the total variance (i.e., in this case, that due only to anomaly experiments) was one to two orders of magnitude smaller than actual differences,$|\Delta_1|$, $|\Delta_2|$ and $|\Delta_3|$. Smaller and less significant values of signal-to-noise ratio were seen later in the day (not shown).

3.3.4 Planetary boundary layer heights and surface fluxes

Again, time series of the domain average differences of sensible and latent heat fluxes for each of the roughness anomaly experiments in the *F* category were analyzed (not shown). As above, the *F* experiments were chosen because of their behavior was representative. It was observed, in this case, that sensible heat fluxes differences ranged from -2.0 to 2.0 W m^{-2} while the corresponding values for latent heat fluxes vary from -3.5 to 4.0 W m^{-2}. In contrast to the previously found behavior for surface fluxes, no clear dependence on roughness length changes for the differences was found. At about 2100 UTC all differences changed from positive to negative and back to positive at about 2300 UTC. The ensemble average of the differences (not shown) showed almost the same time profile, which indicated very little spread within anomaly experiments.

The time behavior of PBL height differences exhibited remarkable similarity to the time evolution of the surface fluxes with negative differences of about -40 m to positive differences of about 20 m. The analysis suggests that PBL height differences in ensemble mean (not shown) is again indicative of very little or no dependence on roughness length changes.

3.4 22 June 2006

3.4.1 Precipitation, wind and thermal response

Positive precipitation differences of up to 20 mm were simulated over northern Illinois while much smaller values of up to 5 mm were for a limited portion of the domain (not shown). The rest of the domain was dominated by negative differences (white regions) that were close to zero. Note that the large precipitation differences between CTRL and CFEN were located in the areas of higher precipitation shown by CTRL (please consult Fig. 3e). Surprisingly, the maximum horizontal wind differences were not found where the largest precipitation differences located. It was also found that the CFEN ensemble experiments produced larger wind speed differences than the CEN and the FEN ensembles over these two regions (not shown). Like the two previously discussed events, there was similarity for the precipitation and horizontal vector field. However, the response to both *C* and *F* roughness changes did have a large impact in wind speed unlike the June 11 and 17 cases. Domain average of precipitation differences (not shown) resulted in values of about 0.05 mm, a factor of 2 smaller than their June 11 and June 17 counterparts.

Precipitation distribution over entire simulation period was quite similar to CTRL. It increased from near zero in the first 12 h of simulation to about 3.7 mm by hour 1200 UTC of 23 June at the end of the simulation. The standard deviations were increased from near zero values to about 1.8 mm near the end. Compared to the 11 June event they were reduced and consistent with values seen in Fig. 3c.

The maximum differences in θ_e for (CTRL−CEN), (CTRL−FEN) (both not shown) and (CTRL−CFEN), are in the order of 10 K and were located over the regions of maximum wind speed differences (not shown). The θ_e differences displayed larger-scale patterns compared to June 11 and 17 with cooler and drier air over northeastern Kentucky and eastern Kentucky–Tennessee border. Interestingly, the magnitude of the difference patterns increased from the CEN ensemble to the CFEN ensemble.

3.4.2 Vertical cross section

As in the horizontal maps, the vertical profiles of θ_e differences showed a progressive increment in magnitude from the CEN, FEN (not shown) and CFEN ensembles that took effect from the surface up to the mixed layer. Downward motion was observed over the southern Kentucky Tennessee border.

3.4.3 Near-surface wind field response

Differences in the domain average of the zonal wind component at 10 m were shown in Fig. 7a for each of the anomaly experiments. For the first 12 h, differences among CTRL and CFDN and CFUP were not detected as was also the case on June 17. After this initial period, anomaly experiments started to deviate from the CTRL. Deviations of anomaly experiments from CTRL were nearly non-existent for the first 12 h of experiments (Fig. 7b). As in other experiments, deviations have become much larger during the last 12 h of experiments. Friction velocity (Fig. 7c) showed a similar pattern as its zonal wind counterpart 12 h into the simulation. In other words, there were very little variations among the differences between anomaly and control simulations. During second 12 h of simulation,

differences showed larger excursions among anomaly experiments but again with no clear tendencies related to roughness length changes.

The statistical significance test was evaluated as in the previous two cases. As in June 17, the values of signal-to-noise ratios were exceedingly large (not shown). The variance during the first 12 h was one to two orders of magnitude smaller than actual differences, $|\Delta_1|$, $|\Delta_2|$ and $|\Delta_3|$. Smaller and less significant values of signal-to-noise ratio were seen later in the day.

3.4.4 Planetary boundary layer heights and surface fluxes

Similar to previous events, changes in PBL height and surface fluxes are very small when compared to CTRL. It was observed, in this case, that sensible heat flux differences ranged from -1.0 to 2.0 W m^{-2} while the corresponding values for latent heat fluxes varied from 1.0 to 4.0 W m^{-2} (not shown). Sensible heat flux differences from the individual experiments were mostly positive from 1800 UTC, except for near-zero values for CFDN05 and CFDN15. There was an apparent tendency for the experiments to cluster around positive values and no clear roughness length dependence was indicated from the results. In contrast, latent heat flux displayed a different behavior, with positive differences from 1800 UTC to 2100 UTC (as sensible heat fluxes) and negative differences after 2100 UTC. Overall, latent heat flux did not show any clear dependence on roughness length changes either. The time behavior of PBL height showed, again, similarity with the time evolution of the surface fluxes for positive differences from about 5.0 to 30.0 m. As discussed previously, PBL height differences in ensemble mean (not shown) was indicative of very little or no dependence on roughness length changes.

4 Discussions and conclusions

The modeled atmospheric response to surface roughness length changes was studied for three synoptic events during June 11, 17 and 22, 2006 over a wide region that included the Ohio–Tennessee River Valley. These assessments were part of an ongoing air quality project. The June 11 case was characterized as a weak frontal event with significant convective activity taking place over central Kentucky. June 17 and June 22 were characterized as prefrontal and frontal events, respectively. These different synoptic conditions played a major role in how the model responded to a wide range of roughness length changes. In all cases, the response showed changes in local precipitation. In ensemble average sense, locally 12-h accumulated precipitation change can be up to 25 mm. On a domain average sense; however, precipitation differences were close to zero due to spatial redistribution of precipitation patterns. This suggests that the model preserved the total amount of precipitation and shifted the location.

The thermodynamic response as evaluated with θ_e also showed similarity of magnitude and pattern for all cases except during the June 22 event where the magnitude of the horizontal and vertical distributions were larger for combined crops and forest change. In ensemble average sense up to 3 K differences were found. The response in the near-surface horizontal wind also differed for June 22 compared to the June 11 and June 17 cases. The former showed a much wider variation in magnitude than the later cases and has the largest increase in wind speed when roughness length changes were performed for the crops and forest combined. The wind speed differences reached up to $\sim$3 m s^{-1}. In addition, with the exception of June 22, the response of the model did not depend on the amount of roughness length change. It was found that small changes in roughness length (e.g., $\pm$5 %) produced magnitude of responses similar to those for larger changes (e.g., $\pm$25 %). This behavior was indicative of the subtle nonlinearities introduced by the change in surface roughness.

The response in the surface energy fluxes and planetary boundary layer height was also examined in the same fashion. The domain average response in surface fluxes varied significantly from event to event and within the ensemble members. The June 11 event displayed a clear dependence on roughness length changes. Both sensible and latent heat fluxes increased as roughness length changed from -25 to 25 %. Additionally, friction velocity showed a clear linear dependence with roughness length that was not found in the June 17 and June 22 events. This was in agreement with what would be expected from the current formulation of the turbulent exchange coefficients in the MM5 for a neutral condition. However, percent change in sensible and latent heat fluxes for this case was too small to be accounted for. The surface fluxes differences for the individual experiments in June 17 and June 22 did not show a clear dependence on roughness length changes as that found for June 11. Rather, June 17 exhibited random variations of these differences. In contrast, the June 22 event showed larger variations in surface energy fluxes with decreased and increased sensible and latent heat fluxes, respectively, compared to the CTRL simulation. Locally, PBL height difference could be between -20 and 40 m. However, the domain average of the PBL height differences exhibited a similar time evolution as that observed for the of the surface energy differences. The results obtained in this study are specific to events where synoptically driven convection or strong prefrontal synoptic conditions were present. Further investigation into events that do not contain these large-scale synoptic

features is still needed to obtain a more detailed and general picture of the sensitivity of the various surface schemes to roughness length.

In summary, the results of this study showed that surface roughness length affects land surface–atmosphere interactions. However, relatively small changes (−25 to 25 %), rather than several order of magnitudes, in roughness length did not modify, in ensemble sense and at least in the range proposed, the amplitude of the response of the model atmosphere as much as expected. This was particularly true for higher and lower most roughness length change scenarios. However, in our opinion, results of this study are important since previous studies mostly focused on large changes in surface roughness length and because this study provided quantitative examples of impacts. In addition, the experimental design of this study and its findings would be quite helpful in the future to better understand the response of the model atmosphere. Furthermore, we suggest that the results are a valuable addition to the meso-scale modeling and roughness literature.

Additional studies involving a variety of land surfaces and synoptic condition combinations are necessary to fully evaluate the importance of roughness lengths on the modeled atmosphere.

Acknowledgments The authors would like to thank two anonymous reviewers and the editor for their valuable comments which helped to improve this paper. Thanks also go to Michael Grogan and Andrew Quilligan for technical assistance. This work is funded by the USDA Grant #58-6445-6-068 and benefited from a NSF Grant #UKRF 3048032200-07-248 and a NSF-EPSCoR grant.

Appendix

The sensitivity of the exchange coefficient (C_h) to changes in roughness length can be approximated using Eq. (26) of Chen and Dudhia (2001) for the neutral case.

$$C_h = \frac{k^2 V_a}{\left[\ln\left(\frac{Z_a}{Z_0}\right)\right]^2} \tag{1}$$

where V_a is the wind speed taken at the lowest vertical computational level, Z_a is the height at that level and Z_o represents the roughness length of both momentum and heat. Keeping V_a constant the sensitivity of C_h is given as:

$$\frac{\Delta C_h}{C_h} = \frac{2}{\ln\left(\frac{Z_a}{Z_0}\right)} \frac{\Delta Z_0}{Z_0} \tag{2}$$

Since Z_a is about 35 m and Z_o for crops/woodland and deciduous broadleaf is 0.2 and 0.5 m, respectively, the above equation can be written approximately for these two categories as:

$$\frac{\Delta C_h}{C_h} = 0.4 \frac{\Delta Z_0}{Z_0} \tag{3}$$

References

Allen T (2006) Flow over hills with variable roughness. Bound Layer Meteorol 121:475–490

Avissar R, Pielke RA (1989) A parameterization of heterogeneous land surfaces for atmospheric numerical models and its impact on regional meteorology. Mon Weather Rev 117:2113–2136

Bottema M, Klaassen W, Hopwood WP (1998) Landscape roughness parameters for Sherwood forest—experimental results. Bound Layer Meteorol 89:285–316

Carruthers DJ, Hunt CR (1990) Fluid mechanics of airflow over hills: turbulence, fluxes, and waves in the boundary layer. In: Blumen W (ed) Atmospheric processes over complex terrain. American Meteorological Society, Boston, pp 83–103

Charney J, Quirck WJ, S-h Chow, Kornfield J (1977) A comparative study of the effects of albedo change on drought in semi-arid regions. J Atmos Sci 34:1366–1385

Chen F, Dudhia J (2001) Coupling an advanced land surface-hydrology model with the Penn State-NCAR MM5 modeling system. Part I: model implementation and sensitivity. Mon Weather Rev 129:569–585

Cheng F, Byun D, Kim S (2003) Sensitivity study of the effects of land surface characteristics on meteorological simulations during the TexAQS2000 period in the Houston–Galveston area, 13th PSU/NCAR Mesoscale Model Users' Workshop, June 10–11, Boulder, CO. ams.confex.com/ams/pdfpapers/80312.pdf

Chervin RM, Schneider SH (1976) On determining the statistical significance of climate experiments with general circulation models. J Atmos Sci 33:405–412

Claussens M (1991) Estimation of aerially-average surface fluxes. Bound Layer Meteorol 54:387–410

De Ridder K, Neirynck J, Mensik C (2004) Parameterising forest edge deposition using effective roughness length. Agric For Meteorol 123:1–11

Dorman JL, Sellers PJ (1989) A global climatology of albedo, roughness length and stomatal resistance for atmospheric general circulation models as represented by the simple biosphere model (SiB). J Appl Meteorol 28:833–855

Dudhia J (1989) Numerical study of convection observed during the winter monsoon experiments using a mesoscale two-dimensional model. J Atmos Sci 46:3077–3107

Eng K, Brutsaert W (2002) How representative are local measurements of the surface shear stress for regional values? Adv Water Resour 25:1349–1355

Finnigan JJ, Shaw RH, Patton EG (2009) Turbulence structure above a vegetation canopy. J Fluid Mech 637:387–424

Garratt JR (1993) Sensitivity of climate simulations to land–surface and atmospheric boundary-layer treatments—a review. J Clim 6:419–448

Garret AJ (1982) A parameter study of interactions between convective clouds the convective boundary layer, and a forested surface. Mon Weather Rev 110:1041–1059

Grimmenes AA, Thue-Hansen V (2004) Annual variation of surface roughness obtained from wind profile measurements. Theor Appl Climatol 79:93–102

Grimmond CSB, Oke TR (1999) Aerodynamic properties of urban areas derived from analysis of surface form. J Appl Meteorol 38:1262–1292

Harman IN (2012) The role of roughness sublayer dynamics within surface exchange schemes. Bound Layer Meteorol 142:1–20

Harman IN, Finnigan JJ (2007) A simple unified theory for flow in the canopy and roughness sublayer. Bound Layer Meteorol 123:339–363

Hassager CB, Nielsen WN, Jensen ON, Boegh E, Christensen HJ, Dellwik E, Soegaard H (2003) Effective roughness calculated from satellite-derived land cover maps and hedge-information used in a weather forecasting model. Bound Layer Meteorol 109:227–254

Hong SY, Pan HL (1996) Nonlocal boundary layer vertical diffusion in a medium-range forecast model. Mon Weather Rev 124:2322–2339

Kain J (2004) The Kain–Fritsch convective parameterization: an update. J Appl Meteorol 43:170–181

Leeper R, Mahmood R, Quintanar AI (2009) Near surface atmospheric response to simulated changes in land-cover, vegetation fraction, and soil moisture over Western Kentucky. Publ Climatol 62(2):41

LeMone MA, Tewari M, Chen F, Alfieri JG, Niyogi D (2008) Evaluation of the Noah Land surface Model using data from a fair-weather IHOP_2002 day with heterogeneous surface fluxes. Mon Weather Rev 136:4915–4940

Lettau H (1969) Note on Aerodynamic roughness-parameter estimation on the basis of roughness element description. J Appl Meteorol 8:829–832

Mahrt L, Ek M (1984) The influence of atmospheric stability on potential evaporation. J Clim Appl Meteorol 23:222–234

McPherson RA, Stensrud VJ (2005) Influences of a winter wheat belt on the evolution of the boundary layer. Mon Weather Rev 133:2178–2199

Mesinger F, Mego G, Kalnay E, Mitchell K, Shafran PC, Ebisuzaki W, Jović D, Woollen J, Rogers E, Berbery EH, Ek MB, Fan Y, Grumbine R, Higgins W, Li H, Lin Y, Manikin G, Parrish D, Shi W (2006) North American regional analysis. Bull Am Meteorol Soc 87:343–360

Oke TR (1987) Boundary layer climates, 2nd edn. Routledge, New York, p 435

Pielke RA (1973) A three-dimensional numerical model of the sea breezes over south Florida. Mon Weather Rev 102:115–139

Pielke RA, Marland G, Betts RA, Chase TN, Eastman JL, Niles JO, Niyogi D, Running SW (2002) The influence of land-use change and landscape dynamics on the climate system: relevance to climate-change policy beyond the radiative effect of green house gases. Philos Trans R Soc 360:1–15

Pitman AJ, Narisma GT, Pielke RA, Holbook NJ (2004) Impact of land cover change on the climate of southwest Western Australia. J Geophys Res 109:D18109. doi:10.1029/2003JDD004347

Quintanar AI, Mahmood R, Loughrin J, Lovahn N (2008) A coupled MM5-Noah land surface model-based assessment of sensitivity of planetary boundary layer variables to anomalous soil moisture conditions. Phys Geogr 29:56–78

Quintanar AI, Mahmood R, Motley MV, Yan J, Loughrin J, Lovahn N (2009) Simulation of boundary layer trajectories dispersion sensitivity to soil moisture conditions: MM5 and Noah-based investigation. Atmos Environ 43:3774–3785

Raupach MR (1994) Simplified expressions for vegetation roughness length and zero-plane displacement as function of canopy area height and area index. Bound Layer Meteorol 71:211–216

Stull RB (1988) An introduction to boundary layer meteorology. Kluwer Academic, Dordrecht

Sud CY, Smith WE (1984) The influence of surface roughness of deserts on the July circulation. Bound Layer Meteorol 33:15–49

Sud YC, Smith WE (1985) Influence of local land-surface on the Indian monsoon: a numerical study. J Clim Appl Meteorol 24:1015–1036

Sud YC, Shukla J, Mintz Y (1988) Influence of land surface roughness on atmospheric circulation and precipitation: a sensitivity study with a general circulation model. J Appl Meteorol 27:1036–1054

Sugita M, Brutsaert W (1992) The stability functions in the bulk similarity formulation for the unstable boundary layer. Bound Layer Meteorol 61:65–80

Thompson RS (1978) Note on the aerodynamic roughness length for complex terrain. J Appl Meteorol 17:1042–1043

Troen I, Mahrt L (1986) A simple model of the atmospheric boundary layer model: sensitivity to surface evaporation. Bound Layer Meteorol 37:129–148

Weligepolage K, Gieske ASM, van der Tol C, Timmermans J, Su Z (2012) Effect of sub-layer corrections on the roughness parameterization of a Douglas fir forest. Agric For Meteorol 162–163:115–126

Wieringa J (1992) Representative roughness parameters for homogeneous terrain. Bound Layer Meteorol 63:323–363

Wu Y, Nair US, Pielke RA, McNider RT, Christopher SA, Anantharaj VG (2009) Impact of land surface heterogeneity on mesoscale atmospheric dispersion. Bound Layer Meteorol 133:367–389

Zehnder JA (2002) Simple modifications to improve fifth-generation Pennsylvania State University-National Center for Atmospheric Research Mesoscale Model performance for the Phoenix, Arizona, Metropolitan Area. J Appl Meteorol 9:971–979

Zhang D-L, Zheng WZ (2004) Diurnal cycles of surface winds and temperatures as simulated by five boundary layer parameterizations. J Appl Meteorol 43:157–169